



# CHORUS

This is the accepted manuscript made available via CHORUS. The article has been published as:

## Nonlinear Frequency Oscillation of Alfvén Eigenmodes in Fusion Plasmas

H. S. Zhang (□□□), Z. Lin (□□□), and I. Holod

Phys. Rev. Lett. **109**, 025001 — Published 10 July 2012

DOI: [10.1103/PhysRevLett.109.025001](https://doi.org/10.1103/PhysRevLett.109.025001)

# Nonlinear Frequency Oscillation of Alfvén Eigenmodes in Fusion Plasmas

H. S. Zhang (张桦森)<sup>1,2</sup>, Z. Lin (林志宏)<sup>2,\*</sup>, I. Holod<sup>2</sup>

<sup>1</sup>Fusion Simulation Center, Peking University, Beijing 100871, China

<sup>2</sup>Department of Physics and Astronomy, University of California, Irvine, CA92697, USA

\*Author to whom correspondence should be addressed. E-mail: zhihongl@uci.edu

## Abstract

A nonlinear oscillation of frequency and amplitude has been found by massively parallel gyrokinetic simulations of Alfvén eigenmodes excited by energetic particles in toroidal plasmas. The fast and repetitive frequency chirping is induced by the evolution of coherent structures in the phase space. The dynamics of the coherent structures is controlled by the competition between the phase space island formation due to the nonlinear particle trapping and the island destruction due to the free streaming. The chirping dynamics provides a conceptual framework for understanding nonlinear wave-particle interactions underlying the transport process in collisionless plasmas.

Energetic particles produced by fusion reactions and auxiliary heating can excite various Alfvén eigenmodes in fusion experiments such as ITER<sup>1</sup>. Associated nonlinear wave-particle interactions can generate significantly enhanced levels of energetic particle transport that would degrade overall plasma confinement and damage fusion devices. Increased energetic particle transport by Alfvén eigenmodes has been correlated<sup>2</sup> with a fast frequency oscillation (chirping) with a sub-millisecond period that has been observed in many experiments<sup>2-6</sup>. In previous studies, an analytic model for the chirping<sup>7,8</sup> based on the one-dimensional (1D) nonlinear wave-particle interaction near marginal stability has been constructed, and a single burst of chirping has been observed in hybrid magnetohydrodynamic simulations with sources and sinks<sup>9</sup>. Here we report the first dynamic observation of fast and repetitive frequency chirping by massively parallel, first-principles kinetic simulations without sources and sinks in a realistic toroidal geometry. The chirping dynamics provides a conceptual framework for understanding the nonlinear wave-particle interaction underlying transport processes in collisionless plasmas. The interaction of energetic particles such as cosmic rays with Alfvén turbulence is also an important issue in space and astrophysical plasmas<sup>10</sup>.

The current simulations using the gyrokinetic toroidal code (GTC)<sup>11</sup> find that the unstable beta-induced Alfvén eigenmodes (BAE)<sup>12</sup> saturate due to nonlinear wave-particle interactions with both thermal and energetic particles. The wave frequency exhibits a fast, repetitive and mostly downward chirping with a sub-millisecond period and a 90° phase shift from the amplitude oscillation. These features have recently been observed in fusion experiments<sup>2</sup>, possibly suggesting a universal dynamics. Analysis of wave-particle interactions shows that the frequency chirping is induced by the evolution of coherent structures in the energetic particle

phase space. The dynamics of the coherent structures is controlled by the competition between the phase space island formation due to the nonlinear particle trapping and the island destruction due to the free streaming process. The nonlinear dynamics and chirping mechanism in the present studies could be applicable to other Alfvén eigenmodes in toroidal geometry with radial variations of mode amplitude and radially asymmetric particle dynamics.

**GTC simulation of BAE**— BAE exists inside a frequency gap of the toroidal Alfvén continuum induced by the plasma beta (ratio of the plasma kinetic pressure to the magnetic pressure). BAE has been routinely observed<sup>3,13-15</sup> in fusion experiments with a significant energetic particle (EP) population. It has strong interactions with both thermal and energetic particles<sup>16-18</sup>. Linear GTC simulations of BAE<sup>19</sup> as well as toroidal and reversed shear Alfvén eigenmodes<sup>20-22</sup> have been verified by theory-simulation comparisons and by benchmarks with hybrid and kinetic simulations. In the current nonlinear GTC simulations, BAE is excited in a tokamak by the EP density gradients near the safety factor  $q = 2$  rational surface located at a minor radius  $r_0 = 0.164R_0$ . Here  $R_0$  is the major radius, the electron density  $n_0$  is uniform, and the EP density at  $r_0$  is  $n_h = 0.01n_0$ . Both thermal and energetic ions are protons with a Maxwellian distribution, and the temperature is taken to be uniform for all species with  $T_e = 0$  and  $T_h = 25T_i$ . Typically  $T_h \sim 10^5 \text{ eV}$  for the fast ions from the neutral beam injection (NBI)<sup>2,3</sup>. The thermal plasma beta at  $r_0$  is  $\beta = 8\pi n_0 T_i / B_0^2 = 0.0072$  with  $B_0$  being the on-axis magnetic field. A filter is applied to keep only a single toroidal mode number  $n=3$  and the poloidal harmonics  $m \in [nq-2, nq+2]$ . Both thermal and energetic ions are governed by nonlinear gyrokinetic equations<sup>23</sup>, and electrons are collectively treated as a linear massless fluid<sup>24</sup>. Coulomb collisions are ignored, and

the parallel electric field is set to zero. Numerical convergences with respect to number of particles, spatial grids, and time steps have been verified.

**Nonlinear saturation and fast chirping**— The nonlinear simulation starts with the small amplitude noise. The BAE mode structure forms around the mode rational surface  $r_0$ , and the amplitude grows with a real frequency  $\omega_{BAE} = 0.96\omega_0$  and a growth rate  $\gamma = 0.09\omega_0$ . Here,  $\omega_0 = \sqrt{(7T_i/2 + 2T_e)/(m_i R_0^2)}$  is the geodesic acoustic mode frequency<sup>16</sup> with  $m_i$  being the proton mass. The linear frequency  $\omega_{BAE}$  is slightly below  $\omega_0$  due to kinetic effects of thermal and energetic ions<sup>19</sup>. The mode amplitude saturates at  $|\frac{e\delta\phi}{T_i}| \sim 10^{-1}$  and  $|\frac{\delta B_r}{B_0}| \sim 10^{-4}$ , where  $\delta\phi$  is the perturbed electrostatic potential and  $\delta B_r$  is the perturbed radial magnetic field. The mode amplitude exhibits a nonlinear oscillation (red curve in Fig. 1a for the  $n=3, m=6$  harmonic at  $r_0$ ) with a period of about ten wave periods, *i.e.*, less than one millisecond for typical experimental parameters. The time evolution of the wavelet power spectrum of the real part of  $\delta\phi$  in Fig. 1b exhibits a regular oscillation of wave frequency  $\omega$ , dominated by mostly downward chirping. For each time step in Fig. 1b, the frequency with the highest power intensity is selected and plotted in Fig. 1a as the black curve. The frequency starts with the linear value of  $\omega_{BAE}$  and chirps downward when the amplitude reaches a high level ( $t \approx 60$ ). Note that the steepest frequency descent occurs when the mode amplitude reaches the maximum, *i.e.*, the amplitude oscillation has roughly a  $90^\circ$  phase lag behind the frequency oscillation. Then the amplitude decreases, and when it reaches a flattened region ( $t \approx 93$ ), the frequency starts to chirp upward. Since the mode amplitude is relatively low during the upward chirping, experimental measurements will mostly see the downward chirping. Overall, there is a small downshift of the wave frequency. All of

these features from our simulations have recently been observed in the NSTX tokamak experiment<sup>2</sup>.

The fast oscillations of wave frequency and amplitude persist without external sources and sinks to replenish the EP distribution function, and the EP density gradients change little after the mode saturation, suggesting the important roles of nonlinear wave and particle dynamics. To delineate the nonlinearity of thermal and energetic ions, two controlled simulations are performed. In one simulation with nonlinear thermal ions and linear energetic ions, the saturation amplitude is similar to Fig. 1, but no oscillations of frequency and amplitude are observed after an initial frequency downshift at the mode saturation. In another simulation with linear thermal ions and nonlinear energetic ions, the mode saturates at the amplitude three times of Fig. 1 and some oscillations of frequency and amplitude are observed. Therefore, the thermal ion nonlinearity is responsible for the BAE saturation and the initial frequency downshift, while the energetic ion nonlinearity is responsible for the frequency chirping.

We examine the mode structures in Fig. 2, which evolve from the linear stage before saturation (panel a), to the nonlinear stage after saturation (panels b and c), and back to the linear-like structure (panel d) when the mode amplitude starts to grow again. A prominent nonlinear feature is the appearance of fine scale structures in the radial direction, which may suggest an important role of mode coupling due to thermal ion nonlinearity in the saturation process<sup>25</sup>. The current simulations ignore coupling between different  $n$  modes, which is expected to be weaker (due to the lack of resonance condition) than self-coupling of a single  $n$  mode. Furthermore, the modes move slightly outward and the mode width decreases from a linear

width of  $0.047R_0$  (defined as full width at half maximum) to a nonlinear width of  $0.031R_0$ . The downward frequency chirping enhances the Landau damping by the thermal ions, especially at the radial edge of the mode amplitude envelope. Therefore, thermal ions cannot be simply represented as a linear damping rate when describing the nonlinear BAE dynamics.

**Dynamics of phase-space structures**— We now examine linear and nonlinear interactions between EP and BAE to elucidate the chirping mechanism. The resonance condition<sup>26</sup> for a low-frequency wave in a general axisymmetric system is  $\omega - k_{\parallel}v_{\parallel} - p\omega_t = 0$  for passing particles, and  $\omega - n\omega_{pre} - p\omega_b = 0$  for trapped particles. Here,  $p$  is an integer number,  $\omega_t$ ,  $\omega_b$ ,  $\omega_{pre}$  are guiding center transit, bounce, and precessional frequencies<sup>27</sup>, respectively. The resonances induce locally large fluctuations of the perturbed distribution function  $\mathcal{F}_h$  in the phase space. The relative strength of resonances can be inferred<sup>28</sup> from the intensity of the EP entropy  $\mathcal{F}_h^2$  as a function of the equilibrium constants of motion ( $E$ ,  $\lambda$ ). Here,  $E$  is the guiding center kinetic energy and  $\lambda = \mu B_0/E$  is a pitch angle parameter with  $\mu$  the magnetic moment. The trapped-passing boundary at  $r_0$  is  $\lambda = 1 - r_0/R_0$ . Four resonances can be identified in both linear and nonlinear stages. The most prominent resonance is the precessional resonance ( $\omega = \omega_d \equiv n\omega_{pre}$ ) of deeply trapped particles. The others include the drift-bounce resonance ( $\omega = \omega_d + p\omega_b$ ) and the second harmonic resonance ( $\omega = 2\omega_d$ ) of trapped particles, and the transit resonance ( $\omega = \omega_t$ ) of passing particles. From linear to nonlinear stage, all resonance regions move to the lower  $E$  while the change in  $\lambda$  is much smaller. Variations of the resonance energy and radial excursions of resonant particles can modify  $\omega_d$  and may induce the wave frequency chirping through mode locking. The dominant radial excursions are associated with the nonlinear particle trapping as

indicated by island-like structures of  $\delta f_h$  at the nonlinear stage with pairs of positive and negative density perturbations.

The dynamics of the dominant precessional resonance can be simply described by a radially local model using canonical variables  $(\zeta, \omega_d)$  with  $\zeta$  the toroidal angle. The evolution of  $\delta f_h/f_{h0}$  in the  $(\zeta, \omega_d)$  phase space is shown in Fig. 3, which is plotted in the linear wave frame moving with an angular velocity of  $\omega_{BAE}/n$  in the EP diamagnetic direction (negative  $\zeta$ -direction). At the linear stage (panel a), wave structures periodic in  $\zeta$  but extended in  $\omega_d$  are formed. The primary precessional resonance appears as the dominant structure at  $\omega_d = \omega_{BAE}$ . A weaker structure at  $2\omega_d = \omega_{BAE}$  indicates the second harmonic resonance. After the saturation (panel b), phase space structures move downward in  $\omega_d$ , and consistently, to the positive  $\zeta$ -direction. Meanwhile, the regions of positive density perturbations (tracked by an “X”) become isotropic and coherent. The regions of negative density perturbations are stretched. In panel (b), the positive regions reach the minimum in  $\omega_d$  ( $\approx 15\%$  below  $\omega_{BAE}$ ), consistent with the wave frequency  $\omega$  chirping downward to the minimum ( $\approx 15\%$  below  $\omega_{BAE}$ ). The negative regions then move upward in  $\omega_d$ , *i.e.*, to the negative  $\zeta$ -direction with respect to the positive regions, and the wave frequency thus starts to chirp upward. The positive regions continue to move to the positive  $\zeta$ -direction and fall below the negative regions (panel c). The mode amplitude now decreases due to a partial cancellation between positive and negative regions when integrating over the velocity space (*i.e.*, phase-mixing). The positive regions shrink in size and continue to move to the positive  $\zeta$ -direction. The mode amplitude then starts to increase as the positive regions pass the negative regions (panel d). When phase space structures become similar to the linear stage, the mode amplitude reaches the

maximum and the wave frequency chirps downward again. The repetitive bursts of mode amplitude and wave frequency chirping persist without external sources and sinks.

The reduced description in Fig. 3 shows that the frequency chirping is induced by the evolution of coherent structures in the precessional resonance region of the  $(\zeta, \omega_d)$  phase space, which propagate at the local  $\omega_d$ . The contribution of other sideband resonances to the evolution of the coherent structures and the frequency chirping is sub-dominant. The  $\omega_d$  variations come from the changes in the kinetic energy  $E$  and the radial excursions of resonant particles. The phase space coherent structures and the oscillations of the mode amplitude both indicate the onset of the nonlinear trapping of resonant particles<sup>29</sup>. However, the trapped particle dynamics in the current simulations is much more complex due to radial variations of mode amplitude and radially asymmetric particle dynamics in the toroidal geometry.

**Nonlinear particle dynamics**— For the precessional resonance that preserves the magnetic moment and the longitudinal invariant in an axisymmetric toroidal system, the nonlinear dynamics of guiding centers can be completely described by a pair of action-angle variables  $(\zeta, P_\zeta)$  with  $P_\zeta = g v_{\parallel} \psi$  the canonical angular momentum,  $2\pi g$  the poloidal current<sup>27</sup>,  $\psi$  the poloidal flux function labeling the radial position  $r$ . We examine the structure of the EP distribution function in the  $(\zeta, P_\zeta)$  space by tracking nonlinear orbits of deeply trapped particles. The particle positions are plotted in the  $(\zeta, P_\zeta)$  space with the color representing the initial  $P_\zeta$  values, which are approximately the radial position since  $P_\zeta \approx -\psi$  for deeply trapped particles.

In the linear phase, when BAE amplitude grows to an appreciable level, resonant particles are strongly perturbed around the mode rational surface (dashed line in Fig. 4). The EP distribution function thus develops a wave-like structure in  $\zeta$  (panel a). As particles move outward (inward) in the radial position  $r$ , the kinetic energy  $E$  decreases (increases) due to the constraint of the longitudinal invariant<sup>30</sup>, and the precessional drift  $\omega_d$  decreases (increases) since  $\omega_d \sim E/r$ . Therefore, the upper (lower)  $P_\zeta$  regions of the structures move to the right (left) and the structures steepen. When the upper  $P_\zeta$  regions move to the opposite phase of the wave, resonant particles originally moving outward are now convected inward and turn around to the left due to the increased  $\omega_d$  (panel b). However, the resonant particles originally moving inward are not all convected outward. Most of them continue to move to the left with the local  $\omega_d$  (*i.e.*, free streaming) to form phase-mixing structures in the lower  $P_\zeta$  region. Therefore, the evolution of the mode structure and the onset of nonlinear particle trapping are not radially symmetric. Particles moving outward (red region in Fig. 4) create positive density perturbation, which form coherent structures (red region in Fig. 3) in the phase space since  $\omega_d$  decreases together with the wave frequency  $\omega$  (*i.e.*, phase locking). On the other hand, particles moving inward (blue region in Fig. 4) create negative density perturbation structures (blue region in Fig. 3), which are distorted quickly since  $\omega_d$  increases (*i.e.*, detuning). This radially asymmetric particle dynamics explains the different evolution of the structures for positive and negative density perturbations in Fig. 3. As the wave frequency chirps downward, the dominant resonance regions in Fig. 4 and the mode structures in Fig. 2 moves outward.

The phase space islands are then formed and the tail of an island (blue region in panel (c) of Fig. 4) moves below another island to the negative  $\zeta$ -direction. The mode amplitude thus

decreases and the  $\omega_d$  increases, *i.e.*, up chirping of the wave frequency. The width of the islands is within the radial domain of  $r/R_0 \sim [0.1, 0.2]$ , which is comparable to the radial mode width in Fig. 2. Therefore the radial variations of the mode amplitude are important to the nonlinear dynamics of resonant particles. The  $P_\zeta$  variations of the coherent structures gives rise to large spreads in  $\omega_d$  that can easily induce the wave frequency chirping range of  $\sim 15\%$ . Finally, the phase space islands<sup>29</sup> in panel (c) quickly become anisotropic structures in panel (d) before trapped particles execute a full rotation. The parts of the islands far away from the mode rational surface are formed by resonant particles moving to the edge of the radial envelope of the mode amplitude. These particles now experience weaker ExB radial convection and thus propagate at the local  $\omega_d$ . The spreads of  $\omega_d$  at each  $\zeta$  location then stretches the islands into fragmented structures (panel d) due to the free streaming process. The associated linear phase-mixing effect is further enhanced by the dependence of the  $\omega_d$  variation rate ( $d\omega_d/d\psi$ ) on the magnetic moment and the longitudinal invariant. These radially nonlocal and multi-dimensional effects lead to the fragmented structures in panel (d), which are drastically different from the picture of the 1D nonlinear Landau damping paradigm<sup>29</sup>. When the positive (negative) region of one structure reaches the positive (negative) region of another structure, the wave amplitude starts to increase to form new islands, which stretch and destroy the structures in panel (d). The cycle of the formation and destruction of coherent structures in the phase space (Fig. 3) thus persists without sources and sinks. The time it takes for an island to stretch in the  $\zeta$ -direction over a distance of the wavelength is the linear phase-mixing time, which defines the life time of the coherent structures and the nonlinear oscillation period of the wave frequency and amplitude. This linear phase-mixing time is typically shorter than the Coulomb collision or turbulence scattering time, which increases with the particle kinetic energy<sup>31</sup>.

Finally, several GTC simulations have been performed to scan the deviation from the marginality. The saturation amplitude is proportional to the square of the growth rate for  $\gamma/\omega_{BAE} < 0.05$  when the phase space island size is smaller than the radial mode width. However, the amplitude is roughly independent of the growth rate for  $\gamma/\omega_{BAE} > 0.08$  when the phase space island size is limited by the radial mode width, as recently observed in NSTX tokamak experiments<sup>32</sup>.

**Acknowledgements:** We acknowledge fruitful discussions with H. Berk, B. Breizman, L. Chen, W. Heidbrink, and F. Zonca. Work is supported by US DOE SciDAC GSEP Center, China Scholarship Council, and National Basic Research Program of China. Simulations were performed using supercomputers at ORNL and NERSC.

#### References:

1. A. Fasoli *et al.*, Nucl. Fusion **47**, S264 (2007).
2. M. Podesta *et al.*, Nucl. Fusion **51**, 063035 (2011).
3. I. G. J. Classen *et al.*, Plasma Phys. Control. Fusion **53**, 124018 (2011).
4. S. D. Pinches *et al.*, Plasma Phys. Control. Fusion **46**, S47 (2004).
5. M. P. Gryaznevich and S. E. Sharapov, Nucl. Fusion **46**, S942 (2006).
6. W. W. Heidbrink *et al.*, Plasma Phys. Control. Fusion **48**, 1347 (2006).
7. H. L. Berk, B. N. Breizman, and H. Ye, Phys. Rev. Lett. **68**, 3563 (1992).
8. B. N. Breizman and S. E. Sharapov, Plasma Phys. Control. Fusion **53**, 054001 (2011).
9. J. Y. Lang and G. Y. Fu, Phys. Plasmas **17**, 042309 (2010).
10. V. S. Ptuskin *et al.*, Astrophys. J. **520**, 204(1999).

11. Z. Lin *et al.*, *Science* **281**, 1835 (1998).
12. A. D. Turnbull *et al.*, *Phys. Fluids B* **5**, 2546 (1993).
13. W. W. Heidbrink *et al.*, *Phys. Rev. Lett.* **71**, 855 (1993).
14. W. Chen *et al.*, *Phys. Rev. Lett.* **105**, 185004 (2010).
15. Z. O. Guimaraes-Filho *et al.*, *Plasma Phys. Control. Fusion* **53**, 074012 (2011).
16. F. Zonca *et al.*, *Plasma Phys. Control. Fusion* **38**, 2011 (1996).
17. P. Lauber *et al.*, *Plasma Phys. Control. Fusion* **51**, 124009 (2009).
18. C. Nguyen *et al.*, *Plasma Phys. Control. Fusion* **51**, 095002 (2009).
19. H. S. Zhang *et al.*, *Phys. Plasmas* **17**, 112505 (2010).
20. W. J. Deng *et al.*, *Phys. Plasmas* **17**, 112504 (2010).
21. W. L. Zhang *et al.*, *Phys. Plasmas* **19**, 022507 (2012).
22. W. Deng *et al.*, *Nuclear Fusion* **52**, 043006 (2012).
23. A. J. Brizard and T. S. Hahm, *Rev. Mod. Phys.* **79**, 421 (2007).
24. I. Holod *et al.*, *Phys. Plasmas* **16**, 122307 (2009).
25. Y. Todo, H. L. Berk, and B. N. Breizman, *Nuclear Fusion* **50**, 084016 (2010).
26. L. Chen, *J. Geophys. Res., [Space Phys.]* **104**, 2421 (1999).
27. R. B. White, *The theory of toroidally confined plasmas.* (Imperial College Press, London, 2006).
28. H. S. Zhang and Z. Lin, *Phys. Plasmas* **17**, 072502 (2010).
29. T. O'Neil, *Phys. Fluids* **8**, 2255 (1965).
30. Y. Xiao and Z. Lin, *Phys. Plasmas* **18**, 110703 (2011).
31. W. L. Zhang, Z. Lin, and L. Chen, *Phys. Rev. Lett.* **101**, 095001 (2008).
32. M. Podesta, private communication, 2012.

**Figure legends:**

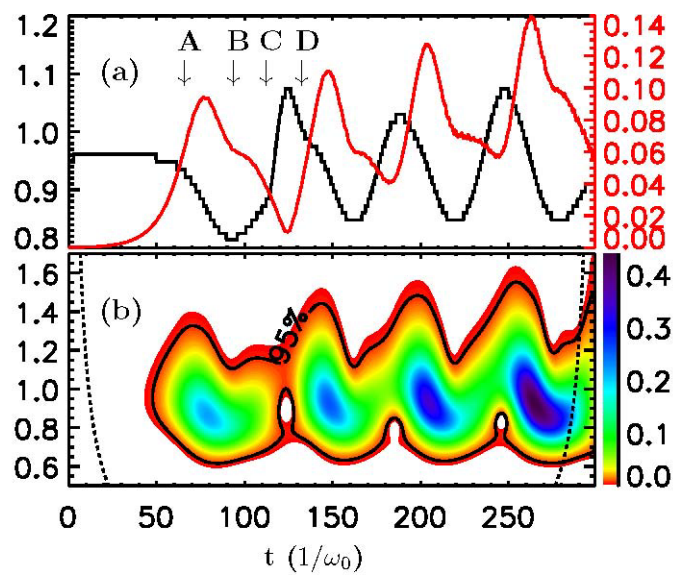


**Figure 1.** Time evolution of (a) BAE amplitude  $|e\delta\phi/T_i|$  (red) and dominant frequency  $\omega$  (black), and (b) frequency power spectrum. The y-axis on the left is  $\omega/\omega_0$ . The unit of the power intensity in panel (b) is arbitrary.

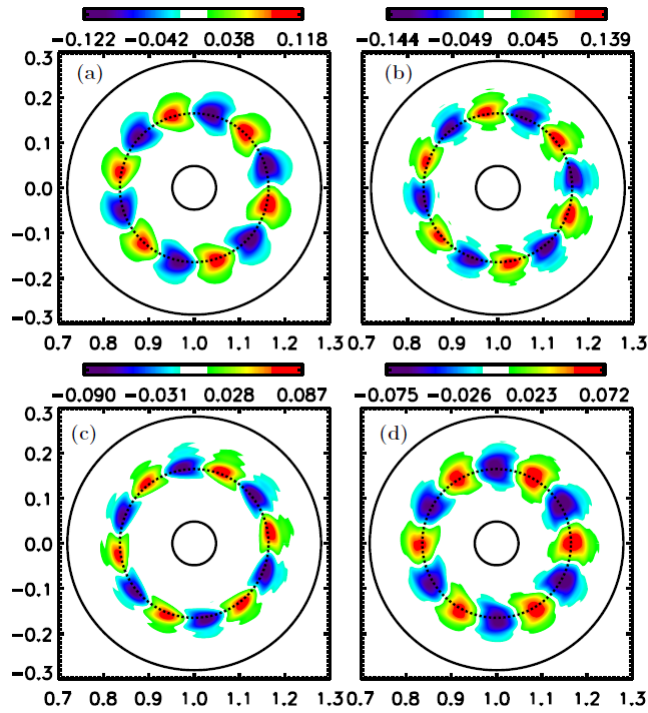


**Figure 2.** Poloidal contour plots of electrostatic potential ( $e\delta\phi/T_i$ ). The dotted circle is the  $r_0$  surface. The x-axis is the major radius  $R/R_0$  and the y-axis is the vertical distance from the mid-plane. Time steps (a)-(d) are labeled by A-D in Fig. 1.

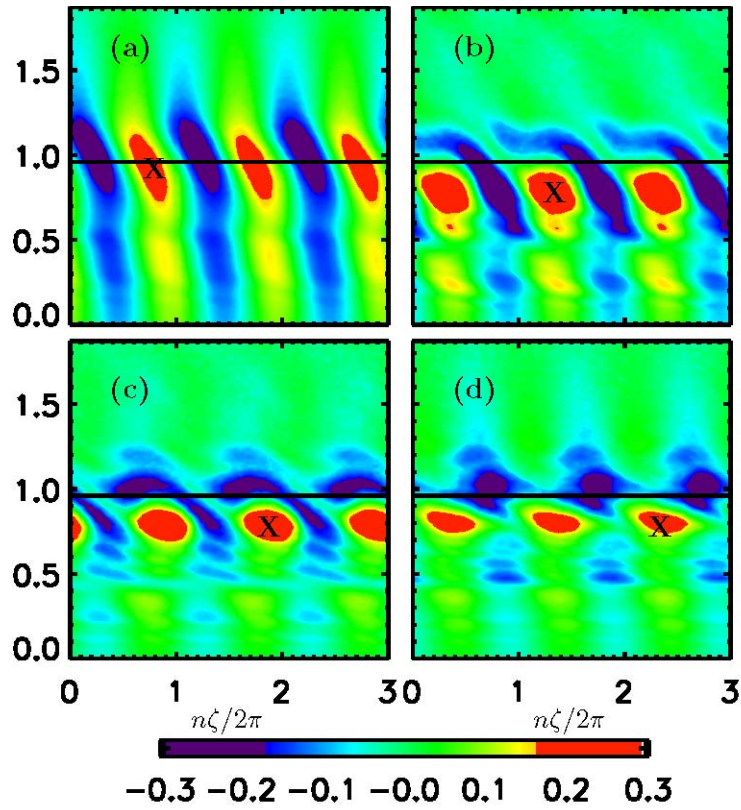


**Figure 3.** Evolution of perturbed distribution function  $\delta f_i/f_{i0}$  in  $(\zeta, \omega_i)$  phase space. The y-axis is  $\omega_i/\omega_0$ . The time evolution is tracked by “X”. Time steps (a)-(d) are labeled by A-D in Fig. 1.

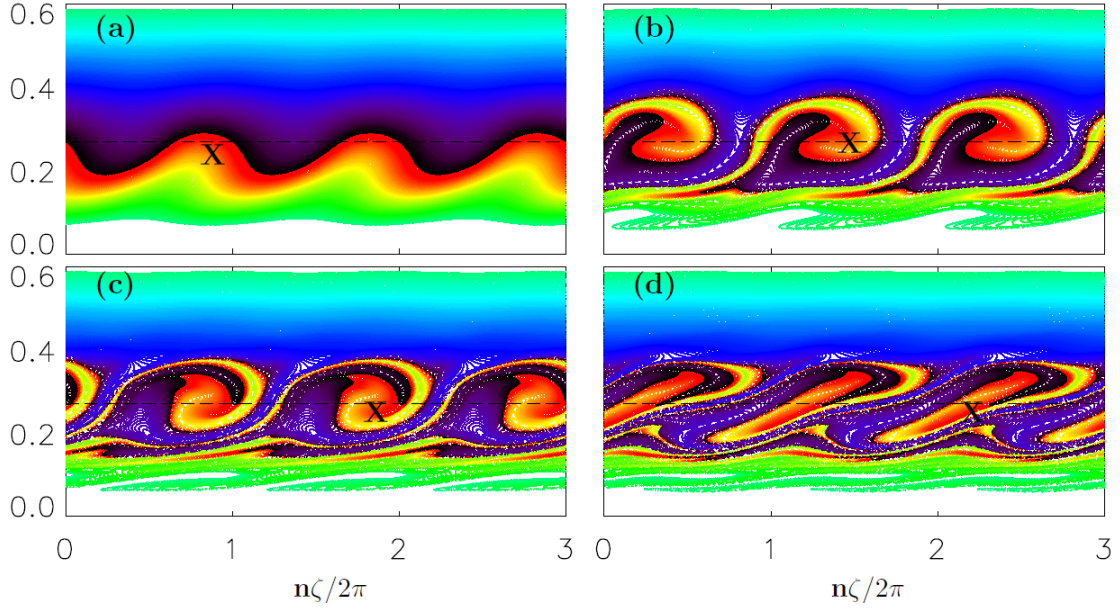


**Figure 4.** Evolution of distribution function in  $(\zeta, P_\zeta)$  space. Particle color represents initial  $P_\zeta$  (normalized by  $-\psi_w$ ). Dashed line represents the mode rational surface. The evolution of an island is tracked by “X”. Time steps (a)-(d) are labeled by A-D in Fig. 1.